Electronic Supplementary Material (ESI) for Nanoscale.

Supporting Information

Electrostatics of metal-graphene interfaces: sharp *p-n* junctions for electron-optical applications

Ferney A. Chaves[1], David Jiménez[1], Jaime E. Santos[2], Peter Bøggild[3], José M. Caridad[3†]

[1]*Department d'Enginyeria Electrònica, Escola d'Enginyeria, Campus UAB, Bellaterra, 08193 Barcelona, Spain*

[2]*Centro de Física and Departamento de Física, Universidade do Minho, P-4710-057 Braga, Portugal*

[3]*Center for Nanostructured Graphene (CNG), Department of Physics, Technical University of Denmark, 2800 Kongens Lyngby, Denmark*

[†]corresponding author: jcar@dtu.dk

Supporting Information Note 1. Numerical calculation of $\phi(r,z)$ and $\sigma(\phi)$ in the device.

We solve the non-linear Poisson's equation, described by Eq. 1, in the *z=0* plane (i.e. the graphene plane) in cylindrical coordinates by a numerical method. The graphene sheet is grounded at a distance far away from the metal-graphene interface. Rotational symmetry is assumed along the azimuthal angle φ and the graphene layer is located between $z = 0$ and $z = t_G$ (Fig.2). The borders

of the calculation region fulfill Neumann-like condition $\frac{d\phi}{d\hat{n}} = 0$ (vanishing electric field, blue dashed lines in Fig. 2b), where $\hat{n}$ is the direction normal to the border, except metal-like borders (red dashed and green dashed-dotted lines in Fig. 2b). Dirichlet-like conditions with a known potential, i.e. $\phi = V_g$ are imposed for the back-gate. Meanwhile, perfect metal (PM) boundary conditions are imposed in the metal island [S1]. This is due to the fact that the island is, in principle, at an unknown potential given by the actual charge of the cluster. The latter depends not only of the charge in the graphene layer, but also on the finite size of the island (i.e. size, shape and density of states, *DOS*) [S2]. For the present study, we consider *p*-*n* junctions where lengths of both *p* an *n* regions are well above the junction width *w*. This is, in our case such junctions are created by thin-film metallic islands on graphene (i.e. cylinders or stripes) with feature sizes (radius or width) > 10 nm. This condition (large cluster size) guarantees the *DOS* of the metal islands to be that one of the bulk metal, as demonstrated below in Note 2.

We further note that to avoid an erroneous calculation of the simulated out-of-plane field, electrostatic potential and junction widths due to Neumann boundary conditions [S3], our simulation region ($\pm r_{max}$, $\pm z_{max}$) is much larger than the calculated widths *w* [S3], at least by an order of magnitude. In particular (Fig. S1), ($\pm r_{max}$ = 250 nm, $\pm z_{max} = t_s$ = 300 nm).

The total free surface density σ depends on the carrier densities in valance *p* band and conduction *n* bands:

$$\sigma = q(p - n). \quad \text{(Eq. S1)}$$

These surface densities *p* and *n* are deduced from the typical linear dispersion of graphene and the Fermi-Dirac thermal distribution and can be expressed in terms of the electrostatic potential ϕ as:

$$n = N_G F_1\left\{\frac{E_F - E_D}{k_B T}\right\} = N_G F_1\left\{\frac{-q\phi}{k_B T}\right\}$$

$$p = N_G F_1\left\{\frac{E_D - E_F}{k_B T}\right\} = N_G F_1\left\{\frac{q\phi}{k_B T}\right\} \quad \text{(Eqs. S2)}$$

Where E_D is the Fermi energy at the Dirac point, q is the elementary charge, k_B is the Boltzmann's constant and *T* is the absolute temperature of the device. $N_G = \frac{2}{\pi}\left(\frac{k_B T}{\hbar v_F}\right)^2$ is the density of states of the graphene sheet, thus, we take into account quantum capacitance effects in the system. These effects may cause [S4] lack of screening at these *p-n* interfaces where the quasiparticle density is very small (see Supplementary Information Note 4). Finally, $F_1(x) = \int_0^\infty \frac{u}{1+e^{u-x}} du$ is the first order complete Fermi-Dirac integral. The solution of the 2D Poisson's equation with the corresponding boundary conditions is obtained by using an algorithm based on the Gauss-Newton iteration scheme applied to the finite element matrix coming from a finite element mesh.

The out of the plane equipotential lines for an exemplary situation corresponding to a symmetric *pn* junction are shown in the Fig. S1. Furthermore, we have considered that the graphene has a thickness of t_G = 0.5 nm and an in-plane relative dielectric permittivity of ε_G = 4 [S5, S6]. Also, the thickness t_d and the relative dielectric permittivity of the dipole layer between the metal and the graphene ε_d, are chosen to be 0.3 nm and the vacuum permittivity ε_0, respectively [S7].

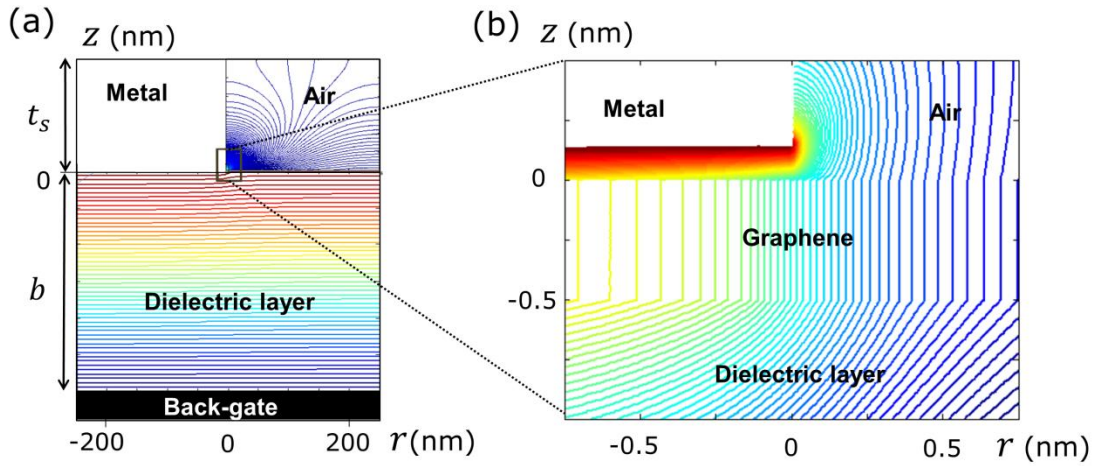

Figure S1. Equipotential lines at metal-graphene interfaces. (a) and (b) Equipotential lines in a graphene device at a metal-graphene interface and surrounding environment in the plane *r*-*z* (the sketch of the device is shown in Fig.2b).

Finally, we have double checked the validity of this electrostatic model for three cases:

(i) Confirming the values of $\Delta E = q\Delta\phi$ given by our model to the thermodynamic stability analysis proposed in Ref [S7]. In both cases $\Delta E \sim$ -0.2 eV for a symmetric lateral *p*-*n* junction created in graphene by Ti as metal (see Fig. 2c, main text and Supporting Information Note 3).

(ii) Confirming that our electrostatic model gives similar junction widths *w* to the ones reported in literature in devices with multiple-gates, for instance, when a lateral *p*-*n* junction created in graphene encapsulated between hexagonal boron nitride (hBN) with a local top gate and a global bottom-gates in the device as done in Ref. [S8]. Incorporating the simulation parameters from Ref. [S8] in our electrostatic model, having a thickness of the top hBN = 15 nm and being the permittivity of this material 3.9, we obtain a $w \sim$ 25nm, very close to the value reported in [S8] (~24nm).

(iii) Verifying our model with experiments. Scanning tunneling microscope (STM) is a high-resolution technique that can be employed to probe accurately the width of p-n junctions created at metal-graphene interfaces [S9]. Sharp *p-n* junctions with potential steps of the order of ~0.1 eV and $w \sim$ 1-3 nm have been measured via scanning tunneling microscopy (STM) in continuous graphene sheets placed on copper [S9], where the differently doped graphene regions occur at the interface of copper surfaces having different surface potentials.

We have performed electrostatic simulations of a graphene sheet on two different metals, configuration showing potential steps of the order of ~0.1 eV, i.e. similar conditions to those reported in Ref. [S9]. Fig. S2 shows the simulated *p-n* junctions with widths ~ 2.8 nm, i.e. very similar to the width measured by STM.

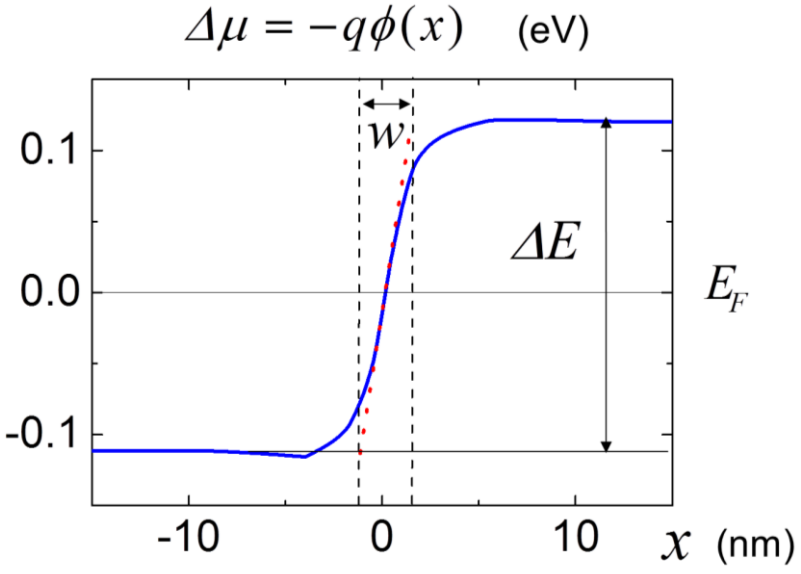

Figure S2. W**idth *w* of lateral *p-n* junctions created in graphene supported by two metals with different surface potentials.** In-plane (z = 0) potential energy $-q\phi(x)$ in the graphene layer across the interface (x = 0) between the first and the second metal. The graphene-metal separation distances in this case are, t_{d1} = 0.3 nm and t_{d2} = 0.5 nm for metals 1 and 2, respectively, similar to

experiments [S9]. In this case, the simulated w = 2.8 nm, a value which is similar to the widths measured via STM [S9].

Supporting Information Note 2. Effect of finite size on the density of states of metal islands.

The level of doping of a graphene sheet in the presence of metal islands in a field effect transistor configuration depends not only on the bulk work functions of the different components of the system (metal,graphene) and the gate voltage applied to the device [S7], but also on a parameter that characterizes the chemical interaction between the graphene sheet and each individual cluster [S2]. Such parameter is subsequently determined by two contributions [S2]: the first one due to the induced surface dipole of graphene and of the metallic islands (together with other components of the system such as gate electrode); and the second one is the correction to the density of states of a cluster due to its finite size and specific shape. In the present study, we consider large metal clusters (i.e. metallic islands), where finite-size corrections to the bulk density of states $DOS(E_F^{Bulk})$ of the metal island at the Fermi level E_F^M do not need to be introduced in our model. We show here that such corrections do not play a major role for metal islands larger than 10 nm. Specifically, considering a spherical metal cluster and using a free-electron gas approximation, finite-size corrections to the bulk density of states are given by [S2] : $DOS\left(E_F^M\right) = DOS\left(E_F^{Bulk}\right) - 3m^* / \left(8\pi\hbar^2 R\right)$, where m^* is the effective mass of the metal atoms. Figure S3 depicts the $DOS(E_F^M)$ of an spherical Ti cluster depending on the radius *R*, showing how $DOS\left(E_F^M\right)$ and $DOS\left(E_F^{Bulk}\right)$ display close values ($DOS\left(E_F^M\right) > 0.96 * DOS\left(E_F^{Bulk}\right)$) for spherical clusters with *R* > 10 nm.

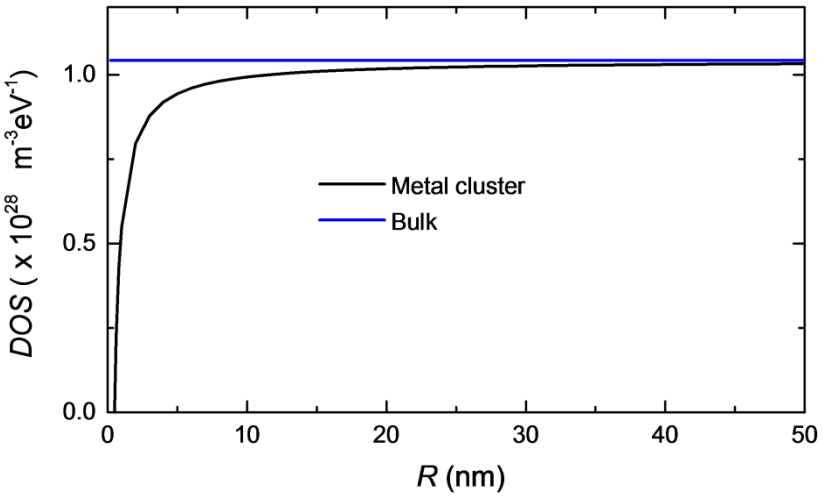

Figure S3. Corrections to the density of states (DOS) of a spherical metallic cluster made from Ti with radius *R*.

Supporting Information Note 3. Estimation of ΔE from a thermodynamic stability analysis.

In order to get a better understanding of the electrostatics of lateral *p*-*n* junctions at metal-graphene interfaces in graphene field-effect devices, we consider a thermodynamic stability analysis of the problem in the two graphene regions: underneath the metal and outside the metal, both of which need to be also in equilibrium with the overall back gate. The model is based on the imposition of thermodynamic equilibrium between the components of the system and allows us to estimate ΔE (or $\Delta\phi$) and to obtain the specific back-gate voltage V_g where a symmetrically doped (bipolar) *p*-*n* junctions is established in the device (i.e. the condition where the Fermi level $E_F = \Delta E / 2$). Before proceeding further, we note that graphene is modelled here as an infinite sheet, not considering finite-size effects such as inhomogeneous gating due to fringing electrostatic fields at the edges of the graphene sheet [S10]. Also, this model is exclusively valid away from the actual lateral junction. We then consider the two graphene regions underneath and outside the metal:

Graphene region underneath the metal

Fig. S4 shows the band diagram of the metal (M), dipole layer (DL), graphene (G), dielectric (D), back-gate (BG) vertical structure [S7,S11], where a *p-type* doped graphene has been assumed as a result of the metal-graphene interaction and the back-gate voltage, without loss of generality. Here W_M, W_G and W_{BG} are the metal, graphene and back-gate work functions, respectively, ΔV_{ox} is the voltage drop across the gate oxide, ΔV the voltage drop across the dipole layer formed between graphene and metal, $\mu_g^{(m)}$ is the Fermi energy variation of graphene underneath the metal, determined as a function of V_G by solving the following set of Eqs. S3. These equations rise from the following conditions: *i)* the total charge density in the vertical heterostructure, including the metal surface charge density Q_M, the graphene layer surface charge density Q_G and the back gate surface charge density Q_{BG} must be zero (Eq.S3a) and *ii)* the sum of voltage drops around any loop (see Fig. S4) from the band diagram should be equal to zero (Eqs.S3b,c):

$$Q_M + Q_G + Q_{BG} = 0 \qquad \text{(Eq. S3a)}$$

$$W_M - q\Delta V - W_G - \mu_g^{(m)} = 0 \qquad \text{(Eq. S3b)}$$

$$W_G + \mu_g^{(m)} + qV_G - q\Delta V_{ox} - W_{BG} = 0 \qquad \text{(Eq. S3c)}$$

As aforementioned, the graphene charge σ below the metal is related to $\mu_g^{(m)} = E_F - E_D$ following the expression $Q_G(\mu_g^{(m)}) = q[p(\mu_g^{(m)}) - n(\mu_g^{(m)})]$. The surface charge densities Q_M and Q_{BG} are related to the voltage drop across the dipole and dielectric layers as $Q_M = -C_d \Delta V$ and $Q_{BG} = C_{ox}\Delta V_{ox}$, respectively; where $C_d = \varepsilon_d / t_d = \varepsilon_0 / t_d$ and $C_{ox} = \varepsilon_2 / b$ describe the dipole layer and back-gate capacitance per unit area. We note that, by performing this infinite parallel-plate capacitor approximation, clusters are assumed to be elongated objects. Combining Eqs. 3, we obtain the

following transcendental equation for $\mu_g^{(m)}$ in graphene below the metal, which is numerically solved.

$$\frac{(C_d + C_{ox})}{q}\mu_g^{(m)} + Q_G(\mu_g^{(m)}) + \frac{C_d}{q}(W_G - W_M) + \frac{C_{ox}}{q}(W_G + qV_G - W_{BG}) = 0 \quad \text{(Eq. S4)}$$

Importantly, we note that this equation is valid for metal islands of any shape, as long as their density of states $DOS\left(E_F^M\right)$ is large (i.e. close to the one of the bulk metal). A more detailed analysis, including finite-size corrections to the bulk density of states $DOS\left(E_F^M\right)$ can be found in [S2].

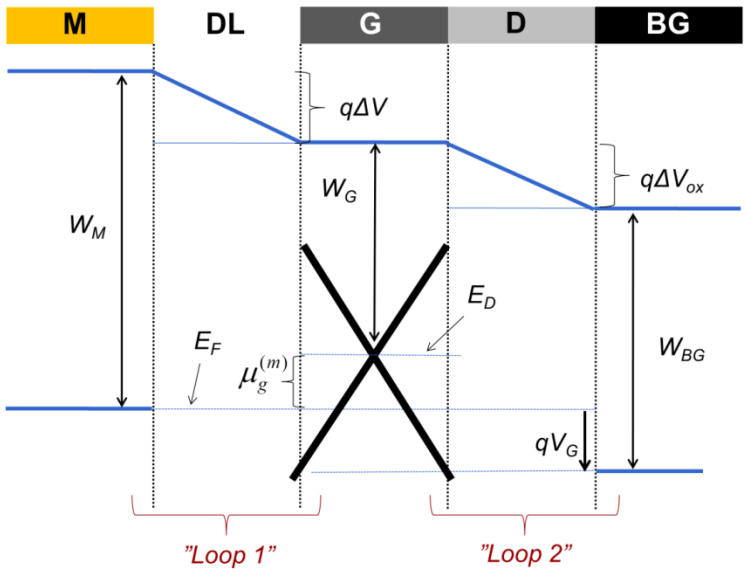

Figure S4. Band diagram of a metal-graphene interface in a gated graphene device. A voltage drop ΔV is produced over the dipole layer (Fig. 2b) and $\mu_g^{(m)}$ represents the shift of the graphene Fermi level E_F with respect to the Dirac point E_D due to both the metal presence and the back-gate.

Graphene region outside the metal

In a similar way, an equation for the shift of the graphene chemical potential outside of the metal region $\mu_g^{(0)}$ and far-away from the lateral junction can be obtained. Outside the metal zone Eq. S3a reduces to $Q_G + Q_{BG} = 0$, Eq S3b is not present and in Eq. S3c, $\mu_g^{(m)}$ is replaced by $\mu_g^{(0)}$. In other words, equilibrium is established between the back gate and graphene only.

Fig. S5 shows the calculated dependence of μ_g on the gate voltage V_g, in both graphene regions below $\mu_g^{(m)}$ and outside $\mu_g^{(0)}$ the metal, far-away from the lateral *p-n* junction. This is done considering titanium (Ti) as the metal, with the following overall parameters [S7,S12]: W_G = 4.5 eV, W_M = 4.33 eV, W_{BG} = 4.5 eV, $\varepsilon_d = \varepsilon_0$, $\varepsilon_2 = 3.9\varepsilon_0$, T = 300 K and b = 300 nm. By comparing both regions, we can see that Ti n dopes graphene and a symmetric *n-p* junction is created when a backgate voltage approximately equal to -10V is applied (condition $\mu_g^{(m)}(V_g) = -\mu_g^{(0)}(V_g)$). Also, the estimated step of the lateral *p-n* junction $\Delta E = -\Delta\mu = q\Delta\phi = \mu_g^{(m)} - \mu_g^{(0)}$ (see Fig.2, main text) is ~ -0.2 eV. Such value is a reasonable match to the -0.28 eV calculated from first principles [S12] and close to the values extracted from experiments, ranging from -0.12 eV [S13] to -0.15 eV [S14]. Furthermore, it is worth noting that values of ΔE from the 1D model accurately agree with those $|\Delta E| = |q\Delta\phi|$ obtained from the 2D model as aforementioned in section S1.

Finally, similar to the electrostatic model, this analysis is applicable to weakly bonded metals, those which do not change the bandstructure of graphene [S2,S7]. We note that, in practice, the strength of metal-graphene coupling (i.e the equilibrium distance metal-graphene) might be complex to determine, not only depending on the type of metal [S7], but also in the deposition conditions, metal granularity or annealing cycles [S14,S15]. Additional information about this can be found in the Note 5 of this Supporting Information.

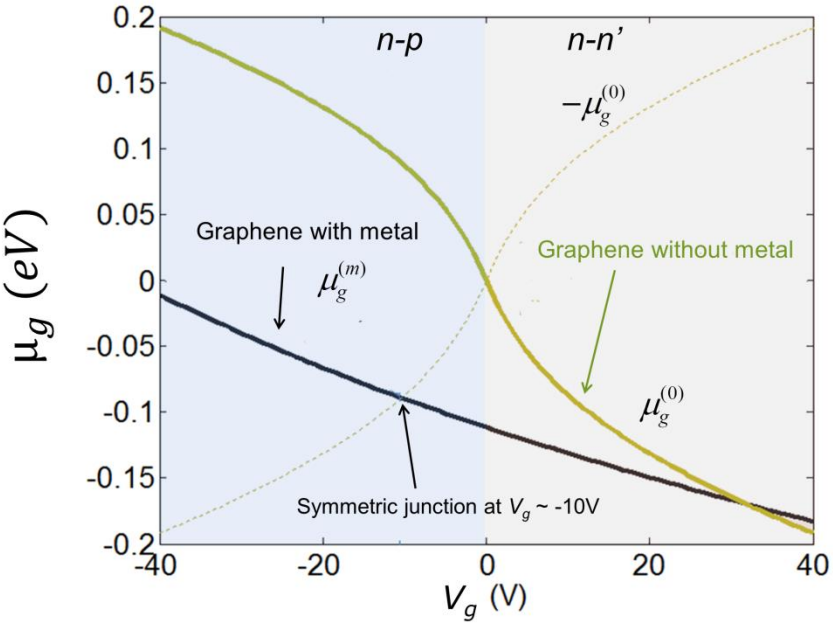

Figure S5. Fermi level of graphene with respect to the Dirac point in regions with and without metal for different gate voltages V_g. Ti is the metal selected for this figure, having a W_M = 4.33 eV. A symmetric and bipolar lateral *n-p* junction is observed in this case for a gate voltage V_g = -10 V.

Supporting Information Note 4. Criterion for treating graphene as a perfect metal at metal-graphene interfaces

In this section, we justify the fact that graphene cannot be considered as a perfect metal to calculate the width of *p-n* junctions *w* at metal-graphene interfaces.

We start from the net current density j_e in a conductor, given by the expression [S16]:

$$j_e = \sigma E - \alpha \nabla \mu \qquad \text{(Eq. S5)}$$

where $\alpha \nabla \mu$ represents the diffusion current. In equilibrium $E = -\nabla \phi$ and $j_e = 0$, $\sigma / \alpha = q$, and we have:

$$\mu + q\phi = const. \qquad \text{(Eq. S5)}$$

At a constant temperature, and if the density of carriers n is close to equilibrium (i.e. $\delta n = n - n^{eq} << 1$), $\nabla\mu = \frac{\partial\mu}{\partial n}\nabla\delta n$ and we can write:

$$j_e = \sigma E - \alpha\frac{\partial\mu}{\partial n}\nabla\delta n \qquad \text{(Eq. S6)}$$

Then, in equilibrium, and using Ficks law $\alpha\frac{\partial\mu}{\partial n} = qD$

$$\nabla\phi + \frac{qD}{\sigma}\nabla\delta n = 0 \qquad \text{(Eq. S7)}$$

where *D* is the diffusion coefficient.

From $\sigma/\alpha = q$ and the fact that $\frac{\partial n}{\partial\mu} \approx DOS(E_F^g)$, $D = \sigma\Big/\left(q^2 DOS(E_F^g)\right)$, which is the Einstein relation [S16]. Hence, using $\delta n = n - n^{eq}$, at the surface of the graphene:

$$\phi + \frac{1}{qDOS(E_F^g)}n = const. \text{ (Eq. S8a)} \quad \text{or} \quad \phi + \frac{\sigma_g}{q^2 DOS(E_F^g)} = const. \text{ (Eq. S8b)}$$

where $\sigma_g = qn$ is the surface charge density in graphene.

On the other hand, σ_g is given by:

$$\sigma_g = -\varepsilon_1\left.\frac{\partial\phi}{\partial z}\right|_{0^+} + \varepsilon_2\left.\frac{\partial\phi}{\partial z}\right|_{0^-} \text{ (Eq. S9),}$$

assuming that graphene is placed at *z=0* and the dielectric constant above and below graphene are $\varepsilon_1 = \varepsilon_{1r}\varepsilon_0$ and $\varepsilon_2 = \varepsilon_{2r}\varepsilon_0$, respectively. For simplicity we take here $\varepsilon_1 = \varepsilon_2 = \varepsilon = \varepsilon_r\varepsilon_0$.

Using Eqs. S8 and S9, we have:

$$\left.\frac{\partial\phi}{\partial z}\right|_{0^+} - \left.\frac{\partial\phi}{\partial z}\right|_{0^-} - \frac{q^2 DOS(E_F^g)}{\varepsilon}\phi = const. \text{ (Eq. S10).}$$

In Eq. S10, one can define the carrier density dependent quantity

$$l_g = \frac{\varepsilon}{q^2 DOS(E_F^g)} \quad \text{(Eq. S11)}$$

which has dimensions of length. l_g represents the scale at which the perfect metal approximation can be used for graphene. In other words, when $l_g = 0$ or, more generally, when l_g is much smaller than any other geometrical lengths in the device, graphene can be considered as perfect metal, and the junction width *w* will be entirely determined by geometrical factors. Otherwise, quantum capacitance effects need to be taken into account in the system due to the lack of screening at *p-n* interfaces [S4]. Here, *w* will be larger, proportional to l_g and dependent on additional parameters including device parameters such as the back gate dielectric and operational parameters such as temperature or carrier density.

In particular, given the density of states of graphene [S17] $DOS(E_F^g) = \frac{2|E_F|}{\pi\hbar^2 v_F^2} = \frac{2\sqrt{\pi n}}{\pi\hbar v_F}$, one can estimate l_g at typical carrier densities of graphene n=10^{12} cm^{-2} to be ~ 0.5 nm when graphene immersed in vacuum $\varepsilon = \varepsilon_0$. As such, first, we cannot use the perfect metal approximation in metal-graphene interfaces, systems where the separation between graphene and metal (~0.3 nm [S7]) is comparable to l_g. Furthermore, we note that l_g not only decreases at lower carrier densities *n* proportionally to $l_g \sim n^{-1/2}$ but also linearly with the permittivity of the surrounding medium ε. This means that the screening of the in-plane electric field at the junction is less effective when increasing the permittivity of the surrounding media [S4], and is one of the reasons why *w* increases when graphene is supported on 'high-k dielectrics' with respect to dielectrics with much lower permittivity (Fig. 3c, main text). We emphasize that the calculated *w* (Figs. 3a and 3c, main text) follows pretty accurately the same trends than l_g: linear with respect to both $n^{-1/2}$ (Fig. 3a) and ε (Fig. 3c).

Supporting Information Note 5. Applicability of our model

Our model is applicable when the interaction between metals and graphene is weak, i.e. the graphene bands, including their conical points at K, are preserved and can be clearly identified. Specifically, this situation occurs when the separation distance between graphene and metal is $t_d >$ 0.3 nm [S7]. Graphene on metals such as Al, Cu, Ag, Au, Pt, show separation distances t_d > 0.3 nm [S7]. Not only that, such situations (t_d > 0.3 nm) also occur for certain configurations of graphene on alternative metals, despite such metals might be commonly regarded to interact strongly with graphene. For instance, this is the case of the so-called "BC" bonding configuration of graphene on Ni [S18].

In addition, we note that the determination of the actual equilibrium distance between metal and graphene t_d (i.e. the strength of the metal-graphene coupling) might be more complex in practice. This will not only depend on the type of metal or equilibrium configuration, but also on device-specific conditions such as vacuum levels when depositing the metal on graphene, metal granularity, performed annealing cycles and/or the formation of a native oxide layer at the interface with graphene in some metals such as Al or Ti [S14, S19, S20]. More generally, we note that even in the case of graphene interacting strongly with some metals, the monolayer could be decoupled from the metallic substrate using different techniques (oxidation, intercalation of different atomic species or others [S21, S22]). All of these comprise examples where graphene's bandstructure will be preserved and thus our model will be applicable.

Supporting Information Note 6. Dependence of the in-plane potential on t_d and ε_d

It is possible to analytically estimate the dependence of the in-plane potential ϕ on the separation distance between metal and graphene t_d and the permittivity of this gap ε_d. Such problem is similar to the calculation of depletion lengths in locally gated field effect transistors made from thin semiconductor films (silicon on insulator, SOI) in order to avoid short-channel effects [S23,S24].

Here, one can show that a natural length λ controls the spread of the potential distribution of $\phi(x)$ in the graphene plane along the x direction (for convenience we use here Cartesian coordinates). Indeed, assuming a simple parabolic form of the potential distribution $\phi(x,z) = c_0(x) + c_1(x)z + c_2(x)z^2$ one can solve the Poisson's equation (Eq.1 main text) with the three boundary conditions of the problem [S23,S24]:

1- $\phi(x,0) = c_0(x)$

2- The electric field at the top of the graphene surface (z = 0, Fig S1b) is determined by the difference between the potentials at metal ϕ_M and graphene $\phi(x,0)$ surfaces and t_d as:

$$\left.\frac{d\phi(x,z)}{dz}\right|_{z=0} = \frac{\varepsilon_d}{\varepsilon_g}\frac{\phi(x,0)-\phi_M}{t_d} = c_1(x)$$

3- The electric field at the bottom of the graphene surface (z = $-t_G$) is close to zero, giving: $c_1(x) - 2t_G c_2(x) \simeq 0$. We note that this approximation is valid when considering a weak field at the supporting dielectric substrate (i.e. no significant backgate potential).

Considering these boundary conditions and a constant graphene permittivity ε_g, Eq.1 can be written as:

$$\nabla^2\phi(x,z) = \frac{\rho_{free}(\phi)}{\varepsilon_g} = \frac{d^2\phi(x,0)}{dx^2} + \frac{\varepsilon_d}{\varepsilon_g}\frac{\phi(x,0)-\phi_M}{t_G t_d} \quad \text{(Eq. 12)}$$

This equation can be solved [S23,S24] by undertaking the transformation $\lambda = \sqrt{\frac{\varepsilon_g}{\varepsilon_d} t_G t_d}$. Indeed, this parameter has units of length and effectively describes the potential distribution $\phi(x)$ of the interface. Without the need to solve the equation, we can clearly see how λ increases when increasing t_d and is proportional to $\varepsilon_d^{-1/2}$. These two trends are observed in our simulations in Figs. 3e and 3f, main text, respectively.

Supporting Information Note 7. Preventing current injection from graphene to metal islands

For a proper functioning of electron-optics devices such as Klein tunneling transistors, current injection from graphene to metal islands should be avoided. This is needed to achieve a large current modulation in these devices.

We undertake a simple resistor circuit analysis (Fig. S6) to quantitatively evaluate the possibility of injecting current from graphene to the floating metal island. As we will see, this calculation incorporates additional device parameters such as metal island size or graphene quality. This information is useful to understand further and design metal-graphene interfaces for electron-optics applications.

Here, we assume for simplicity that *i)* the sheet resistance of graphene underneath the metal R_g^M is similar to the sheet resistance of the graphene without metal on top R_g^0: $R_g^M = R_g^0 = R_g^S$ (i.e. we solve the symmetric junction case). Furthermore, in this case, *ii)* the metal on top of graphene is a rectangle, width W = 1 μm and length L_M, dimensions which are larger than the current injection/ejection region L_i from graphene to metal and viceversa ($L_i = \sqrt{\rho_C / R_g^S}$ where ρ_C is the contact resistivity at the metal-graphene interface. [S25].

Based on this simple circuit, the current flowing through graphene underneath the metal I_g with respect to the incident current I_{in} is $I_g / I_{in} = 1/\left(1 + R_g / 2R_c\right)$ and takes values 84% and 96.2% for L_M = 0.5 μm and L_M = 100 nm, respectively. The former calculations have been performed assuming a graphene sheet with mobility μ = 20000 $cm^2V^{-1}s^{-1}$ at a carrier density $n = 2\times10^{12}$ cm^{-2} ($R_g^S = (ne\mu)^{-1} \sim 150\Omega$), and typical contact resistivities at metal-graphene interfaces $\rho_c \sim 1\times10^{-5}$ Ωcm^2 [S11, S26]. For both calculated cases L_i is limited by L_M ; and the graphene and contact resistances are given by the expressions $R_g = R_g^S L_M / W$ and $R_c = \sqrt{\rho_c R_g^S}\coth\left(L_M / L_i\right)/W \approx \sqrt{\rho_c R_g^S}/W$.

We note that these values are consistent with values calculated using a more advanced resistor networks model [S27], where > 75% of current flowing through graphene with a lower mobility μ = 5000 $cm^2V^{-1}s^{-1}$ for a length L_M = 1 μm. In general, the larger ρ_c and the shorter L_M , the higher percentage of current flows through graphene. As such, this ratio can be controlled and custom tailored by increasing the distance between metal and graphene t_d (using the aforementioned techniques described in Supporting Note 5) since ρ_c increases exponentially when increasing t_d , see Ref. [S26].

Finally, we note that the estimated current ratio values are consistent with experiments [S13] demonstrating the creation of electron optics devices by depositing metallic dots with sizes ~100 nm on graphene transistors with mobilities μ ~ 20000 $cm^2V^{-1}s^{-1}$.

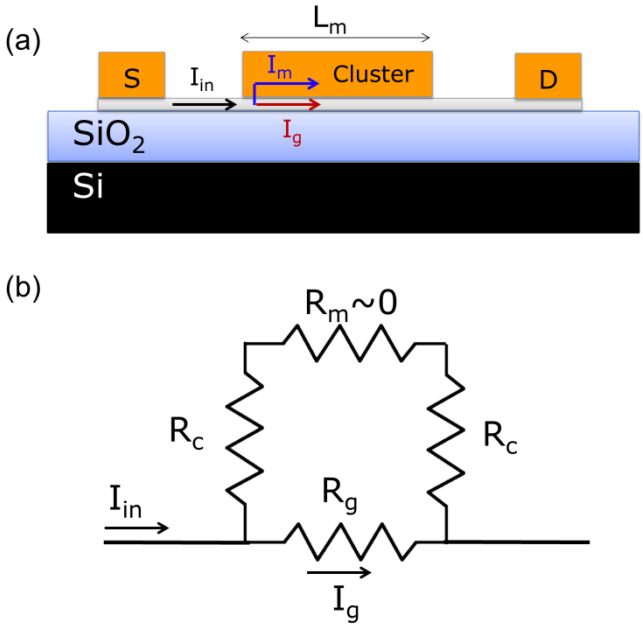

Figure S6. (a) Schematic of the device with the floating metal cluster of length L_m on the graphene channel. (b) Equivalent circuit model, approximating the metal resistance R_m to zero.

Supplementary References

S1. A. Konrad and M. Graovac. The finite element modeling of conductors and floating potentials. IEEE Transactions on Magnetics, 32, 5, 4329, 1996.

S2. J.E. Santos, M.M.R. Peres, J.M.B. Lopes dos Santos and A. H. Castro Neto. Electronic doping of graphene by deposited transition metal atoms. Phys. Rev. B 84, 085430 (2011)

S3. A. Nipane, Y. Zhang and J. T. Teherani. Role of out-of-plane dielectric thickness in the electrostatic simulation of atomically thin lateral junctions. *J. Appl. Phys.* 123, 214032 (2018).

S4. L.M. Zhang and M.M. Fogler. Nonlinear screening and ballistic transport in graphene p-n junction. *Phys.Rev.Lett.* 100, 116804 (2008).

S5. E.J.G. Santos and E. Kaxiras. Electric-Field dependence of the effective dielectric constant in graphene. *NanoLett.* 13, 3, 898 (2013).

S6. M. v Schilfgaarde and M.I. Katsnelson. First-principles theory of nonlocal screening in graphene. Phys. Rev. B 83, 081409 (2011)

S7. G.Giovannetti, P.A. Khomyakov, G. Brocks, V.M. Karpan, J. van den Brink and P.J. Kelly. Doping graphene with metal contacts. *Phys. Rev. Lett.* 101, 026803 (2008).

S8. G-H. Lee, G-H. Park and H-J. Lee. Observation of negative refraction of Dirac fermions in graphene. Nat. Physics. 11, 925 (2015)

S9. K.K. Bai, J-J. Zhou, Y-C. Wei, J-B. Qiao, Y-W Liu, H-W. Liu, H. Jiang and L. He. Generating atomically sharp p-n junctions in graphene and testing quantum electron optics on the nanoscale. *Phys. Rev. B*, 97, 045413 (2018).

S10. J.M. Caridad, S.R. Power, M.R. Lotz, A.A. Shylau, J.D. Thomsen, L. Gammelgaard, T.J. Booth, A-P. Jauho and P. Bøggild. Conductance quantization suppression in the quantum Hall regime. Nature. Comm. 9, 659 (2018).

S11. F.A. Chaves, D. Jiménez, A.A. Sagade, W. Kim, J. Riikonen, H. Lipsanen and D. Neumaier. A physics-based model of gate –tunable metal-graphene contact resistance benchmarked against experimental data. 2D Mater. 2, 025006 (2015)

S12. Q. Ran, M. Gao, X. Guan, Y. Wang and Z. Yu. First-principles investigation on bonding formation and electronic structure of metal-graphene contacts. *Appl. Phys. Lett.* 94, 103511 (2009)

S13. J.M. Caridad, S. Connaughton, C. Ott, H.B. Weber and V. Krstić. An electrical analogy to Mie scattering. *Nat. Commun.* 7, 12894 (2016)

S14. M. Zhu, J. Wu, Z. Du, S. Tsang, E.H.T. Teo. Gate voltage and temperature dependent Ti-graphene junction resistance toward straightforward p-n junction formation. *J. Appl. Phys.* 124, 215302 (2018).

S15. Q. Wilmart, A. Inhofer, M. Boukhicha, W. Yang, M. Rosticher, P. Morfin, N. Garroum, G. Feve, J.-M. Berroir and B. Placais. Contact gating at GHz frequency in graphene. Sci. Rep. 6, 21085 (2016)

S16. C. Kittel. Introduction to Solid State Physics. *John Wiley & Sons*.

S17. H.Yu, A. Kutana and B.I. Yakobson. Carrier delocalization in two-dimensional coplanar p-n junctions of graphene and metal dichalcogenides. *NanoLett*., 16, 5032 (2016).

S18. V.M. Karpan, G. Giovanetti, P.A. Khomyakov, M. Talanana, A.A. Starikov, M. Zwierzycki, J. van den Brink, G. Brocks and P.J. Kelly. Graphite and graphene as perfect spin filters. *Phys. Rev. Lett*. 99, 176602 (2007)

S19. D. Mann, A. Javey, J. Kong, Q. Wang and H. Dai. Ballistic transport in metallic nanotubes with reliable Pd ohmic contacts. *NanoLett.* 3, 11, 1541, (2003)

S20. C. Gong, S. McDonnell, X. Qin, A. Azcati, H. Dong, Y.J. Chabal, K. Cho and R.M. Wallace. Realistic metal-graphene contact structures. *ACSNano* 8, 642, (2014)

S21. P. Matyba *et al*. Conrolling the electronic structure of graphene using surface-adsorbate interactions. *Phys. Rev. B.* 92, 041407 (2015)

S22. I. Palacio *et al*. Chemistry below graphene: decoupling epitaxial graphene from metals by potential-controlled electrochemical oxidation. *Carbon*. 129, 837 (2018)

S23. R-H. Yan, A. Ourmazd and K.F. Lee. Scaling the Si MOSFET: From bulk to SOI to Bulk. *IEEE Trans. Elect. Dev*. 39, 7 (1992).

S24. J.P. Colinge. Multiple-gate SOI MOSFETs. *Solid State Electronics* 48, 897, (2004).

S25. K. Nagashio and A. Toriumi. Density-of-States Limited Contact Resistance in Graphene Field-Effect Transistors. *Jpn. J. Appl. Phys*., 50, 070108, (2011).

S26. F.A. Chaves, D. Jiménez, A.W. Cummings and S. Roche. Physical model of the contact resistivity of metal-graphene junctions. *J. Appl. Phys*. 115, 164513 (2014)

S27. K. Nagashio, T. Moriyama, R. Ifuku, T. Yamashita, T. Nishimura and A. Toriumi. Is graphene contacting with metal still graphene?. *IEEE International Electron Devices*, DOI: 10.1109/IEDM.2011.6131475